

Fermi LAT gamma-ray observations of the supernova remnant HB 21

G.Pivato

University and INFN Padova, via Marzolo 8, 35131 Padova, Italy

J.W.Hewitt

NASA Goddard Space Flight Center, Greenbelt, MD 20771, USA

L.Tibaldo

KIPAC - SLAC, MS 29,2575 Sand Hill Rd., Menlo Park, CA 94025, USA

on behalf of Fermi LAT collaboration

We present the analysis of Fermi Large Area Telescope (LAT) γ -ray observations of HB 21, a mixed-morphology supernova remnant. Such supernova remnants are characterized by an interior thermal X-ray plasma, surrounded by a wider nonthermal shell emitting at radio frequencies. HB 21 has a large angular size, making it a good candidate for detailed morphological and spectral studies with the LAT. The radio extension is $2^\circ \times 1^\circ 5'$, compared to the LAT 68% containment angle of $\sim 1^\circ$ at 1 GeV. To understand the origin of γ -ray emission, we compare LAT observations with other wavelengths that trace non-thermal radio synchrotron, nearby molecular clouds, shocked molecular clumps, and the central X-ray plasma. Finally, we model possible hadronic and leptonic emission mechanisms. We conclude that γ -rays from HB 21 are likely the result of electron bremsstrahlung or proton-proton collisions with dense material due to interaction with the nearby clouds.

1. INTRODUCTION

HB 21 (also known as G89.0+4.7, Green [2009]) is a mixed morphology (MM) supernova remnant (SNR) interacting with molecular clouds. X-rays observations with *Einstein* provide evidence that the supernova (SN) explosion took place in a low-density cavity, therefore suggesting a massive stellar progenitor (Knoedlseder et al. [1996]). HB 21 is located in a dense environment with a radio shape suggestive of interactions with the nearby clouds (Byun et al. [2006]). Looking at the CO distribution it is possible to distinguish two different structures based on the velocity of the molecular clouds. Koo and Heiles [1991] report the presence of broad CO lines emitted from shocked clumps of molecular gas with high column densities. The distance to HB 21 was first estimated to be 0.8 kpc from ROSAT X-rays observations (Leahy and Aschenbach [1996]). Considering the preshock velocities, the X-ray absorbing column densities, the relation between photometric distance of Hii region and velocity of molecular clouds and the highly polarized emission, the distance was later determined to be ~ 1.7 kpc (Byun et al. [2006]).

High-energy γ -ray sources coincident with HB 21 were reported in the 2-years Catalog of the Large Area Telescope (LAT) on board the *Fermi Gamma-ray Space Telescope* (Nolan et al. [2012]). Three sources are associated with the remnant (2FGL J2043.3+5105, J2046.0+4954, and J2041.5+5003) and an additional source lies on the edge (2FGL J2051.8+5054). Due to the large apparent size ($\sim 2^\circ$) this object is well suited for a detailed morphological study with *Fermi* LAT. Here we present the analysis of ~ 4 years of LAT observations of HB 21 and the discussion of the γ -ray emission mechanism in light of archival multiwavelength observations. In §2 we describe our morphological

and spectral characterization of the γ -ray emission from HB 21, the sources of systematic errors and the strategy adopted to estimate them. In §3 the interpretation of these results is finally discussed. This paper is intended to be a summary of the poster we presented at Fermi Symposium. For a detailed description of the analysis and a more comprehensive discussion of the results we defer the reader to the paper in preparation Pivato et al. [2013].

2. FERMI LAT DATA ANALYSIS

For this analysis, we use data accumulated from the beginning of scientific operations, on 2008 August 4, to 2012 June 14, selecting the low-background event class P7SOURCE_V6. For the morphological characterization we use only events with energy > 1 GeV to profit from the narrower point-spread function (PSF) in order to separate the γ -ray emission associated with HB 21 from neighboring sources and interstellar emission. We then use events down to 100 MeV to determine the spectral energy distribution of the remnant. Below this threshold the PSF becomes much broader than the SNR and the uncertainties related to the instrument response are larger. In both the morphological and spectral characterization we consider photons with measured energies up to 300 GeV, but only find a significant detection of the source up to energies of several GeV due to the limited number of events at high energies.

We perform the analysis in a $10^\circ \times 10^\circ$ region of interest (RoI) centered at the radio position of HB 21 ($l=89^\circ 0'$, $b=+4^\circ 7'$). The background is composed of diffuse emission and individual nearby γ -ray sources. Diffuse emission is taken into account using the standard models provided by the *Fermi* LAT collabora-

arXiv:1303.2091v2 [astro-ph.HE] 12 Mar 2013

tion. We include in the background model all the point sources present in the 2FGL catalog Nolan et al. [2012] with distances less than 15° from the RoI center and which are not associated with the SNR. We will discuss in §2.1 the case of the source 2FGL J2051.8+5054, which is located at the edge of the SNR. The spectral model used for background sources is that reported in the 2FGL catalog. Fluxes and spectral indices are left as free parameters in the fit if the source is within the RoI. Otherwise they are fixed to the catalog values.

Two major sources of systematic errors on the results are the uncertainties in the LAT effective area and the modeling of interstellar emission. The uncertainties in the effective area for the IRFs we use are evaluated as 10% at 100 MeV, 5% at 516 MeV, and 10% above 10 GeV, linearly varying with the logarithm of energy between those values (Ackermann et al. [2012]). We estimate the error induced in the characterization of the γ -ray emission spectrum from HB 21 by repeating the analysis with two sets of modified IRFs where the effective area was upscaled or downscaled by its uncertainty. To gauge the systematic uncertainties due to the interstellar emission model we compare the results obtained using the standard model with the results based on eight alternative interstellar emission models (de Palma et al. 2013).

2.1. Morphological study

In Figure 1a we show a count map of the RoI for energies > 1 GeV, to visually illustrate the morphology of the γ -ray emission in the region.

We compare the morphology in γ rays with that in the radio (see figure 2a) and an X-ray band (see figure 2b). As shown in figure 2b the γ -ray emission is broader than the X-ray (ROSAT) emitting plasma. Figure 2a shows that γ emission well compares with radio shell even if it extends beyond the radio shell in region where CO clouds are present. Furthermore, note that the brightest part of γ -ray emission coincides with known shocked molecular clouds (labelled S1, S2, and S3 in figure 2c).

To characterize the morphology in the γ -ray band we approximate the SNR with a disk, for which we determine from γ -ray data the best-fit center position and radius. We considered both the cases where 2FGL J2051.8+5054 is included as a separate point source in the model or removed. The significance of the separate source hypothesis is below the threshold usually required to claim a detection for LAT sources so we do not consider 2FGL J2051.8+5054 as a separate source and, therefore, we remove it from the model. The best fit parameter in this case are: $l=88.75\pm 0.04$, $b=4.67\pm 0.05$, $r=1.19\pm 0.05$. Errors reflect statistical uncertainties only. We note that the results concerning HB 21 are robust regardless of

whether 2FGL J2051.8+5054 is included as a separate source in the model or not.

When the alternative interstellar emission models are used, the γ -ray disk is systematically shifted toward the north-western part with respect to the radio shell (with shifts in longitude between $0^\circ 19$ and $0^\circ 24$, and in latitude between $0^\circ 06$ and $0^\circ 09$), and the disk radius is systematically smaller by $0^\circ 18$ – $0^\circ 24$. We note that, as for the standard model, for all the alternative models the disk extends beyond the rim of the remnant in coincidence with the western molecular cloud.

2.2. Spectral study

Modeling HB 21 with the best-fit disk we determine the spectrum over the full energy range. We study the spectral shape of the γ emission in the energy range between 100 MeV and 300 GeV. We compare a curved spectrum

$$\frac{dN}{dE} = N_0 \left(\frac{E}{1000 \text{ MeV}} \right)^{-(\alpha + \beta \ln(E/1000 \text{ MeV}))}$$

with a power law. We obtain that the curved spectrum is preferred at 9σ , so now on our spectral shape in all energy range will be the log-parabola. Using the log-parabolic function, the total energy flux from HB 21 at energies above 100 MeV is 9.4 ± 0.8 (stat) ± 1.6 (syst) $\times 10^{-11}$ erg cm $^{-2}$ s $^{-1}$ and the photon flux 1.48 ± 0.2 (stat) ± 0.4 (syst) $\times 10^{-11}$ ph cm $^{-2}$ s $^{-1}$.

We also computed the spectral energy distribution (SED) in a model-independent way by splitting the full energy range in 12 logarithm-spaced bins. We show the resulting SED in Figure 3. Systematic errors related to the modeling of interstellar emission are obtained repeating the analysis using the alternative models and extracting the root mean square of the variations with respect to the values from the standard model. Those values are then summed in quadrature with the error due to the LAT effective area uncertainties for display. At energies below a few hundred MeV the systematic errors are driven by the uncertainties related to the modeling of interstellar emission because the broad PSF reduces the source to background ratio. The effective area uncertainties have a comparable or larger impact at higher energies.

3. SPECTRAL ENERGY DISTRIBUTION MODELING

To constrain the particle distribution we simultaneously fit radio (Leahy [2006]) and γ -ray emission from nonthermal electrons and protons. We adopt the simplifying assumption that all emission originates from a region characterized by a constant mat-

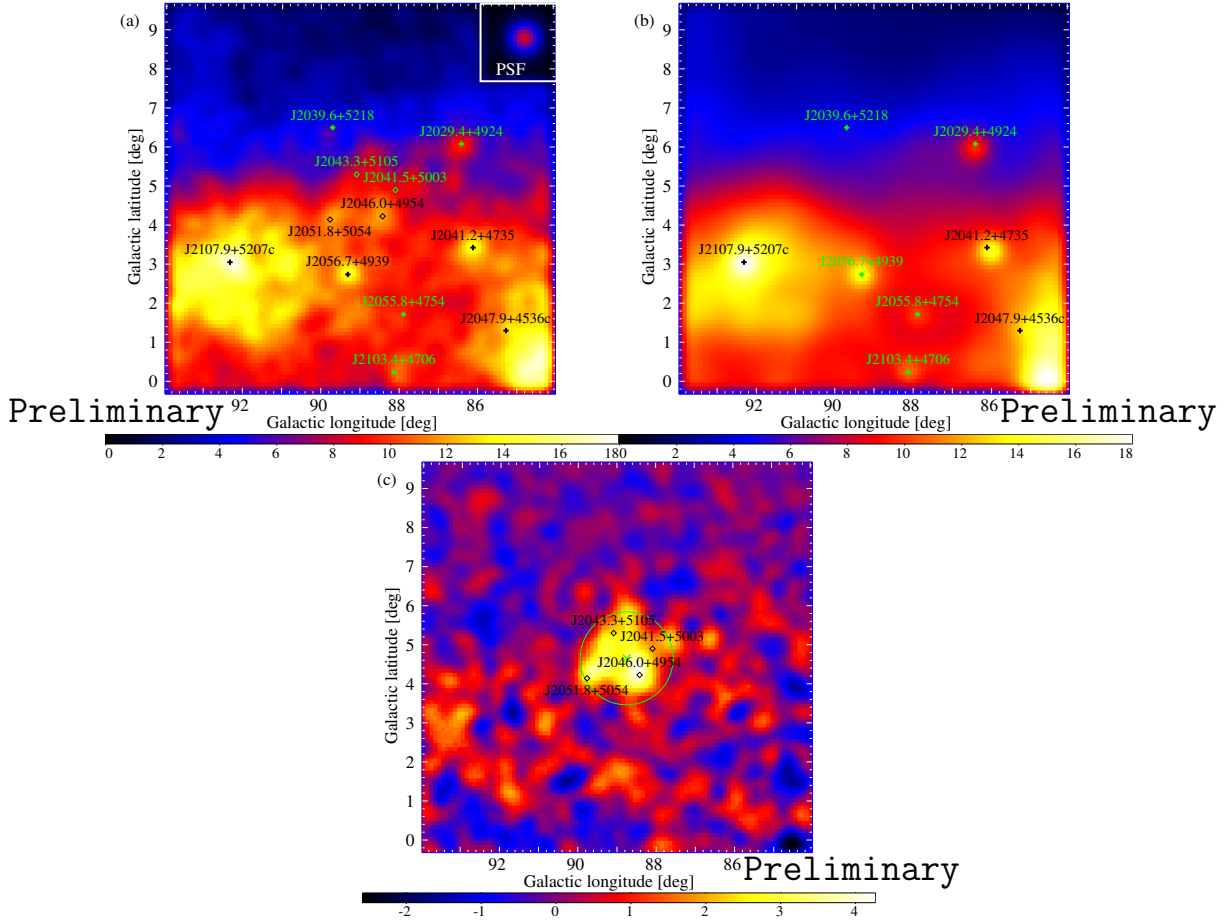


Figure 1: a) LAT counts map at energies > 1 GeV. We overlaid the positions of 2FGL sources (crosses for background sources and diamonds for the three sources associated with the remnant and 2FGL J2051.8+5054). The inset in the top right corner shows the effective PSF over the energy range considered for a power-law spectral distribution with index 3.1. b) Background model map (calculated using the fit parameters for the case when HB 21 is modeled using the best-fit disk). c) Remaining emission associated with HB 21; overlaid are the positions of the four point sources above and the best-fit disk. The pixel size is $0^\circ.1$ and all maps are smoothed for display with a Gaussian kernel of $\sigma=0^\circ.4$.

ter density and magnetic field strength. This single emitting zone is assumed to be equal to the size of the remnant derived from the best-fit gamma-ray disk. The particle spectra are assumed to follow a power-law with an exponential cutoff of the form $dN/dE \simeq \eta_{e,p} E^{-\Gamma} \times \exp(E/E_{max})$, with the same spectral index and energy cutoff for both electrons and protons.

The radio index, α , is related to the γ -ray photon index, Γ , by $\Gamma = 2\alpha + 1$ for bremsstrahlung or pion-decay models, giving $\Gamma = 1.76$ (We note that for this particle index, both a cutoff and a spectral break by an index of one give an equally valid fit). Modeled spectral energy distributions (SEDs) are presented in 4. Model parameters are given in Table I. We also give the total energy of accelerated particles integrated above 1 GeV for protons, and above 511 keV for electrons. While the chosen parameters are not unique in their ability to fit the broadband spectrum, they are representative.

Table I One-Zone Model Parameters

Model	Γ	p_{max} [GeV/c]	n_H [cm^{-3}]	B_{tot} [μG]	η_e/η_p	W_p [erg]	W_e [erg]
IC	1.76	200	0.1	3	1	1×10^{49}	4×10^{49}
Brems.	1.76	4	10	100	0.1	5×10^{48}	4×10^{49}
π^0 -decay	1.76	6	10	100	0.01	2×10^{49}	1×10^{48}

The energetics implied by nonthermal models are in line with those determined with other old SNRs in a dense environment. Regardless of the dominant emission mechanism, the energetic requirement is for $\sim \text{few} \times 10^{49}$ ergs. The hadronic model indicates $\sim 2 \times 10^{49}$ erg in accelerated cosmic ray protons and nuclei. Leptonic models require $\sim 4 \times 10^{49}$ ergs in electrons. SNR HB 21 is known to be interacting with molecular clouds, and a moderately enhanced aver-

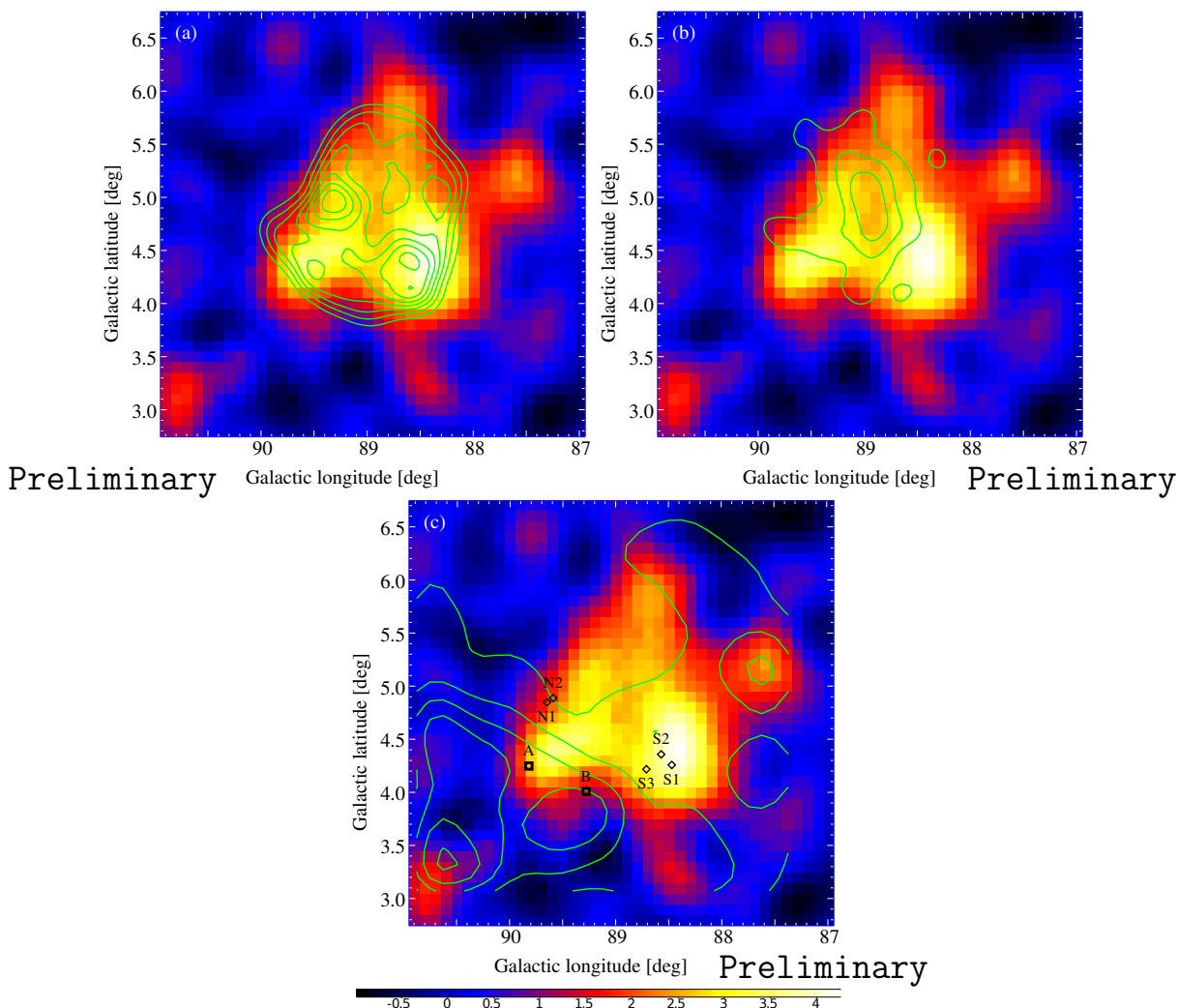


Figure 2: Emission associated with HB 21 (Fig. 1c) overlaid with contours from emission at other wavelengths: a) Radio emission intensity at 6 cm from Sino-German Telescope [Gao et al. 2011]. Data were smoothed with a Gaussian kernel of $\sigma=0.2$. The seven contour levels are linearly spaced from 0 Jy beam⁻¹ to 2.0 Jy beam⁻¹. b) Background-subtracted X-ray emission smoothed with a Gaussian kernel of $\sigma=0.25$. The three contour levels are linearly spaced from 0.36×10^{-3} to 2.13×10^{-3} counts s⁻¹ arcmin⁻². c) Intensities of the 2.6 mm CO line in the Local-Arm region. The six contour levels are linearly spaced from 1.5 K km s⁻¹ to 28 K km s⁻¹. We also show the positions of the shocked CO clumps and clouds A and B given in Koo and Heiles [1991].

age density would favor hadronic or bremsstrahlung models for γ -ray emission. The IC-dominated model requires a low density ($N_H \leq 0.1$ cm⁻³) to prevent bremsstrahlung emission from dominating. Such a density is unreasonably low for HB 21. Interestingly, HB 21 has an uncharacteristically low luminosity compared to other γ -ray SNRs known to be interacting with molecular clouds. The total luminosity of the HB 21 above 100 MeV at a distance of 1.7 kpc is 4×10^{34} erg s⁻¹, while most interacting SNRs, such as IC 443 have luminosities of 10^{35} erg s⁻¹ or greater. It is possible that the lower luminosity of HB 21 is due to a lower total mass of the molecular clouds with which it is known to be interacting.

4. CONCLUSIONS

We analyzed the γ -ray measurements by the *Fermi* LAT in the region of HB 21, a mixed-morphology SNR. We detect significant emission ($\sim 29\sigma$ associated with the remnant). The emission is best modeled by a disk centered at (l,b)=(88°62±0°05,+4°79±0°06) with a radius $r=1°19 \pm 0°06$ (statistical uncertainties only), so it is well resolved by the LAT for energies greater than 1 GeV. The γ -ray emission extends over the whole area of the non-thermal radio shell, larger than the X-ray emitting thermal core. The emission in γ -rays may extend beyond the radio shell in a region rich of interstellar matter in the north western part of the SNR. Furthermore, the brightest γ -ray emit-

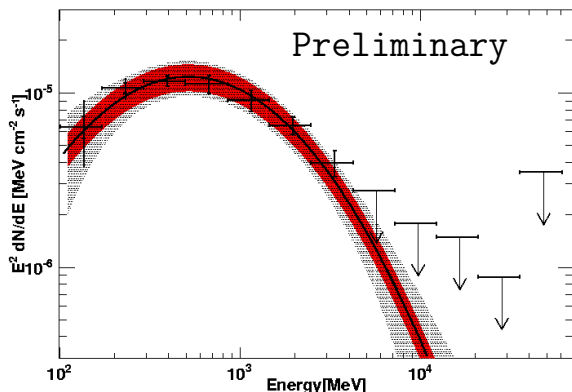


Figure 3: Spectral energy distribution (SED) of HB 21. The line shows the best-fit log-parabola model, the light filled area shows the statistical error band and the gray area shows the systematic uncertainties. For the points error bars correspond to statistical errors only, while lines show the larger systematic errors. 95% confidence-level upper limits are given for energy bins where the TS of the source is < 9 .

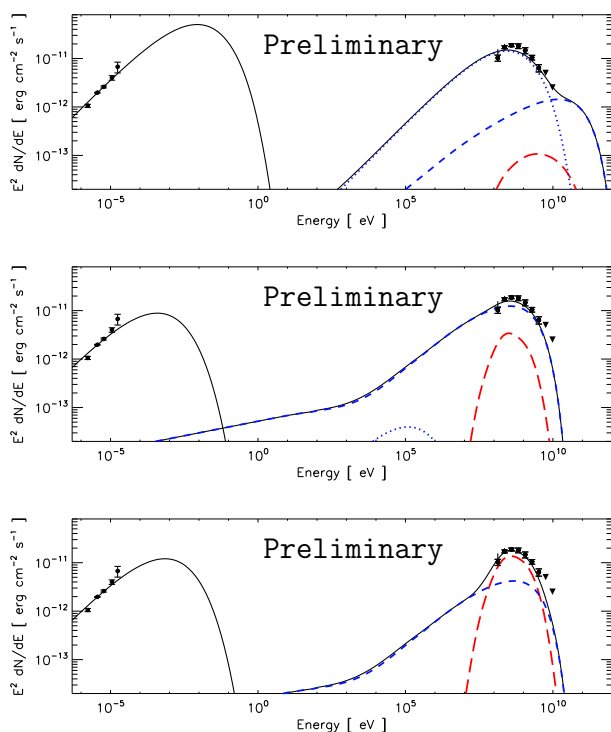


Figure 4: SED models for which IC (top), bremsstrahlung (middle) and π^0 -decay (bottom) are the dominant emission mechanism. In each model the radio data are fit with a synchrotron component, shown as a black curve. The individual contributions of π^0 -decay (long dashed), bremsstrahlung (short dashed), and IC emission from CMB (dotted) are shown. The sum of the γ -ray emission is shown by the solid curve. The leptonic and hadronic components are colored blue and red, respectively.

ting region coincides with known shocked molecular clumps. Both results are suggestive that collisions of shock-accelerated particles with interstellar matter are responsible for the observed γ -ray emission.

The spectrum is best modeled by a curved function, indicative of a cutoff or break in the spectrum of the accelerated particles, typical of middle-aged SNRs in a dense interstellar environment. The total γ -ray luminosity of HB 21 above 100 MeV is estimated to be $\sim 4 \times 10^{34}$ erg s^{-1} , fainter than other SNRs interacting with MC detected by the LAT. This can be explained by the lower mass of the molecular clouds supposed to be in interaction with the remnant. The γ -ray emission may be dominated either by π^0 decay due to nuclei or by Bremsstrahlung from energetic electrons. An IC origin is disfavored because it would require unrealistically low interstellar densities in order to prevent Bremsstrahlung to dominate. Based on the most likely values for the ISM densities over the volume of the remnant, in the hadronic-dominated scenario accelerated nuclei contribute a total energy of $\sim 2 \times 10^{49}$ ergs. In the leptonic-dominated scenario we need accelerated electrons for $\sim 4 \times 10^{49}$ ergs, and also nuclei for $\sim 10^{49}$ ergs. Such energy densities match those required to make SNRs the dominant source of the Galactic CRs [e.g. O’C. Drury 2012]. Recently, Reichardt et al. [2012] perform an analysis on HB 21 using 3.5 years of *Fermi* LAT data. The conclusions are in agreement with those presented in this proceeding if we consider that we adopt a distance from HB 21 of 1.7 kpc (according to Byun et al. [2006]) instead of 0.8 kpc adopted in earlier works and based on the association with the Cygnus OB7 complex. In particular our values of flux and luminosity of the SNR are in agreement. Finally they assume a density of 60 cm^{-3} which is the maximum density estimation. Instead, we consider both the minimum and the maximum possible densities obtaining that the energy accelerated particles is $\sim 0.3 - 4 \times 10^{49}$ erg, regardless of whether hadronic or leptonic emission is dominant. Finally, in our work also systematic effects due to interstellar emission model and effective area are taken into account.

Acknowledgments

The *Fermi* LAT Collaboration acknowledges support from a number of agencies and institutes for both development and the operation of the LAT as well as scientific data analysis. These include NASA and DOE in the United States, CEA/Irfu and IN2P3/CNRS in France, ASI and INFN in Italy, MEXT, KEK, and JAXA in Japan, and the K. A. Wallenberg Foundation, the Swedish Research Council and the National Space Board in Sweden. Additional support from INAF in Italy and CNES

in France for science analysis during the operations phase is also gratefully acknowledged.

Work supported by Department of Energy contract DE-AC03-76SF00515.

References

- D. A. Green, Bulletin of the Astronomical Society of India **37**, 45 (2009), 0905.3699.
- J. Knoedlseder, U. Oberlack, R. Diehl, W. Chen, and N. Gehrels, A&AS **120**, C339 (1996), arXiv:astro-ph/9604057.
- D.-Y. Byun, B.-C. Koo, K. Tatematsu, and K. Sunada, ApJ **637**, 283 (2006).
- B.-C. Koo and C. Heiles, ApJ **382**, 204 (1991).
- D. A. Leahy and B. Aschenbach, A&A **315**, 260 (1996).
- P. L. Nolan, A. A. Abdo, M. Ackermann, M. Ajello, A. Allafort, E. Antolini, W. B. Atwood, M. Axelsson, L. Baldini, J. Ballet, et al., ApJ Supplement **199**, 31 (2012), 1108.1435.
- G. Pivato, J. W. Hewitt, L. Tibaldo, T. Brandt, F. de Palma, F. Giordano, G. Jhannesson, D. A. Smith, and al. (2013), in preparation.
- M. Ackermann, M. Ajello, A. Allafort, W. B. Atwood, M. Axelsson, L. Baldini, G. Barbiellini, D. Bastieri, K. Bechtol, R. Bellazzini, et al., Astroparticle Physics **35**, 346 (2012), 1108.0201.
- F. de Palma, F. Acero, T. J. Brandt, F. Giordano, J. W. Hewitt, G. Johannesson, L. Tibaldo, and J. Ballet (2013), these Proceedings.
- X. Y. Gao, J. L. Han, W. Reich, P. Reich, X. H. Sun, and L. Xiao, A&A **529**, A159 (2011), 1102.4503.
- D. A. Leahy, ApJ **647**, 1125 (2006).
- L. O'C. Drury, Astroparticle Physics **39**, 52 (2012), 1203.3681.
- I. Reichardt, E. de Ona Wilhelmi, J. Rico, and R. Yang, A&A **546**, A21 (2012), 1207.2057.